Check for updates

Original Research Article

Cynaropicrin Alleviates Pulmonary Embolism in Rats by Inhibiting the MEK/ERK/Egr-1/TF Signaling Pathway, Suppress Inflammatory Pathways, and Apoptotic Cascades

Pharmacognosy Magazine
22(2) 679–689, 2026
© The Author(s) 2025
Article reuse guidelines:
in.sagepub.com/journals-permissions-india
DOI: 10.1177/09731296251362994
journals.sagepub.com/home/phm
Sage

Kaimin Lu[1] and Mingliang Wu[1]

Abstract

Background: Cynaropicrin (CYN) exhibits anti-inflammatory and anti-thrombotic properties, but its effects on pulmonary embolism (PE) are poorly understood.
Objectives: This study aimed to investigate the effects of CYN on PE induced by autologous blood clots in a rat model and to explore the underlying mechanisms.
Materials and Methods: Forty male Wistar rats were divided into four groups: sham, PE, PE + 10 mg CYN, and PE + 25 mg CYN. CYN's impact on inflammatory factors and coagulation was assessed using hematoxylin and eosin (H&E) staining and enzyme-linked immunosorbent assay (ELISA) for oxidative stress (OS) and inflammatory markers (tissue factor (TF), monocyte chemoattractant protein-1 (MCP-1), vascular cell-adhesion molecule-1 (VCAM-1), and intercellular adhesion molecule-1 (ICAM-1)). Real-time polymerase chain reaction (PCR) analyzed the MEK/ERK/early growth response protein 1 (Egr-1)/TF signaling pathway, while immunohistochemistry (IHC) examined caspase-3 and p53 expression in lung tissue.
Results: CYN treatment significantly reduced body and lung weights in the PE groups ($p < .05$). Serum levels of inflammatory markers were elevated in the PE group but decreased with CYN treatment ($p < .05$). OS markers improved with CYN, and gene expression of MEK/ERK pathway components was reduced ($p < .05$). CYN also led to dose-dependent decreases in apoptosis markers (caspase-3, p53). Structural improvements in lung tissue were observed via stereological and transmission electron microscopic (TEM) analyses.
Conclusion: CYN demonstrated therapeutic effects by inhibiting inflammation and suppressing the MEK/ERK/Egr-1/TF signaling pathway. Further research is warranted to confirm these findings and assess CYN's safety and efficacy in humans.

Keywords

Apoptosis, MEK/ERK/Egr-1/TF, antithrombotic agent, pulmonary embolism, cynaropicrin

Received 19 February 2025; **revised** 16 April 2025; **accepted** 02 June 2025

Introduction

Pulmonary embolism (PE) is associated with a notably high death rate, making it the third most prevalent cardiovascular disease. It has a grim outlook, with respective death rates of 13% and 26% at 1 month and 1 year post-diagnosis, and presents a significant threat to patients' lives (Freund et al., 2022). Chronic thromboembolic pulmonary hypertension (CTEPH) can develop as a long-term complication of pulmonary hypertension (PH), following thromboembolism, causing sustained blood flow obstruction and subsequent intimal remodeling and thickening of the small pulmonary arteries (Kim et al., 2019). According to Mercier et al. (2022), in CTEPH patients, pulmonary artery endothelial cells (PAECs) may stimulate the proliferation of pulmonary artery smooth muscle cells (PASMCs) and facilitate monocyte migration through the paracrine signaling of cytokines and growth factors, thereby worsening fibrotic changes within the vascular structure. The

[1]Department of Respiratory and Critical Care Medicine, Affiliated Hospital of Shaoxing University, Shaoxing, Zhejiang, China

Corresponding author:
Mingliang Wu, Department of Respiratory and Critical Care Medicine, Affiliated Hospital of Shaoxing University, Shaoxing, Zhejiang 312000, China.
E-mail: wumingliang0575@outlook.com

Creative Commons Non Commercial CC BY-NC: This article is distributed under the terms of the Creative Commons Attribution-NonCommercial 4.0 License (http://www.creativecommons.org/licenses/by-nc/4.0/) which permits non-Commercial use, reproduction and distribution of the work without further permission provided the original work is attributed as specified on the SAGE and Open Access pages (https://us.sagepub.com/en-us/nam/open-access-at-sage).

MEK/ERK signaling pathway, part of the mitogen-activated protein kinase (MAPK) cascade, plays a crucial role in transmitting signals from growth factors and hormones to the nucleus, involving key components such as MEK, ERK, and the transcription factor early growth response protein 1 (Egr-1). This pathway is activated by pro-inflammatory stimuli and growth factors, leading to increased expression of procoagulant factors like tissue factor (TF), which is essential for thrombus formation (Barbosa et al., 2021). Additionally, the MEK/ERK pathway is vital for vascular smooth muscle cell proliferation and migration, aiding in vascular repair and angiogenesis by promoting endothelial cell activity through growth factors like vascular endothelial growth factor (VEGF). It interacts with other pathways, such as the PI3K/Akt, to amplify responses to growth factors and inflammation (Dai et al., 2021).

Cynara scolymus L., commonly recognized as artichoke, is one of the oldest plants renowned for its medicinal properties. According to liquid chromatography-electrospray ionization-tandem mass spectrometry assays, this plant is rich in isoflavonoids, including biochanin A, daidzein, formononetin, and luteolin (Salekzamani et al., 2019; Zaker-Esteghamati et al., 2021). A key bioactive compound in artichoke extracts is cynaropicrin (CYN), a sesquiterpene lactone that activates the Nrf2 pathway (Gonçalves et al., 2023). Prior studies have shown that CYN inhibits the nuclear factor kappa-light-chain-enhancer of activated B cells (NF-κB) transcriptional activation pathway and possesses many beneficial effects, such as anti-inflammatory, anti-tumor, antioxidant, anti-parasitic, anti-photoaging, and anti-hyperlipidemic activities (De Cicco et al., 2021).

CYN improves PH through modulating various signaling pathways. It can explicitly inhibit SphK1-mediated NF-κB activation, which results in decreased proliferation of PASMCs and mitigates muscular changes in pulmonary vessels (Li et al., 2024). Research by Liu et al. (2022) highlights that CYN curbs PASMC proliferation through the regulation of the miR-638/NR4A3/cyclin D1 axis (Liu et al., 2022; Porro et al., 2024). In terms of its anti-inflammatory properties, CYN has been noted to inhibit the MAPK pathway and the monocyte chemoattractant protein-1 (MCP-1) expression in cases of PE, while also lowering mean pulmonary artery pressure (mPAP) in PE rats. Beyond its anti-inflammatory effects, CYN significantly improves endothelial function, alleviates oxidative stress (OS), and decreases the expression of nicotinamide adenine dinucleotide phosphate (NADPH) oxidase in small pulmonary arteries affected by monocrotaline in rats. Nonetheless, there is no research on the CYN effects on PAECs in the context of CTEPH or on human-derived PAECs (Matos et al., 2021).

We assessed the impact of CYN on PE caused by autologous blood clots injected into the pulmonary arteries via a right jugular vein model, while also investigating the underlying mechanisms involved.

Materials and Methods

Animals

Forty adult Wistar rats (220 ± 30 g; 3 months old) were kept in propylene cages at 23°C ± 2°C, with a lighting cycle including 12 h of light and 12 h of darkness. The rats underwent a 72-h adaptation period in the laboratory to aid their acclimatization before the CTEPH model induction. Animals could drink water and eat rat pellets, in accordance with the ethical standards and protocols established by the ethics committee of Shaoxing University Hospital. Animals were then randomly allocated to one of four groups: sham, PE, PE + 10 mg/kg CYN, and PE + 25 mg/kg CYN. A dosage of 10 mg of CYN was dissolved in normal saline (0.5 mL) and administered to the treatment groups. For the induction of CTEPH, thromboembolism is achieved using autologous blood clots or a thrombin solution, injecting the thrombus into the right pulmonary artery, typically in a volume of 0.5 mL, depending on the rat's size, followed by the closure of the thoracotomy in layers to ensure proper hemostasis. Postoperative care includes monitoring the rats until they regain consciousness, providing analgesics such as buprenorphine for pain management, and observing for any signs of distress or respiratory difficulties. Finally, an assessment of CTEPH is conducted at 2-, 3-, and 4-weeks post-surgery. Furthermore, CYN was injected intraperitoneally at 10 and 25 mg/kg/day for 4 weeks, 1 h before the CTEPH protocol (Wu et al., 2020; Ye et al., 2023).

Enzyme-linked Immunosorbent Assay (ELISA) Assay

After administering pre-anesthesia with xylazine 2% (100 mg/kg; Sigma, USA), followed by anesthesia using ketamine 10% (15 mg/kg; Sigma, USA), anesthetization was done. Blood sampling was done from the ophthalmic vein plexus and stored at 4°C. The supernatant collection was done through centrifugation. The concentrations of TF, interleukin-6 (IL-6), vascular cell-adhesion molecule-1 (VCAM-1), interleukin-1 beta (IL-1β), MCP-1, and intercellular adhesion molecule-1 (ICAM-1) in the peripheral blood of the rats were assessed, following the instructions provided with the ELISA kit (R&D Systems, USA). Optical density (OD) was evaluated at 450 nm by an Eon spectrophotometer (BioTek Instruments, USA). The experimental procedures were conducted three times as recommended (Gao et al., 2018).

Acute Toxicity Test (Lethal Dose 50 (LD_{50})) for CYN

Lork's two-step method determined the least toxic and most effective dose of CYN. First, nine animals were assigned to three groups of three rats and given intraperitoneal injections of CYN at 1, 10, and 100 mg/kg. Three more animals were

allocated to three various groups, receiving CYN at 2, 20, and 200 mg/kg through the same administration route. After observing for 24 h, the LD_{50} of CYN was determined by the below equation:

$$LD_{50} = (A \times B)/2$$

A denotes the lowest dose that resulted in toxic symptoms like skin rashes, diarrhea, death weight loss, or nausea in the group, while B signifies the highest dose without fatalities or toxic symptoms (Dibua et al., 2022).

Lung Tissue Total Antioxidant Capacity (TAC)

First, 50 mg lung tissue samples were collected from each rat and placed in ice-cold phosphate-buffered saline (PBS; homogenization buffer). The tissue was then cut into smaller pieces (1–2 mm) by a scalpel or sterile scissors. Next, the pieces were located in a Dounce homogenizer with the homogenization buffer at a typical ratio of 1:10 (tissue to buffer) and homogenized on ice to prevent degradation. After homogenization, the homogenate was transported to microcentrifuge tubes and received centrifugation at 4°C for 10–15 min at 10,000–15,000 × *g* to eliminate debris and intact cells. The supernatant, which contains the homogenized tissue extract, was carefully collected. Finally, the homogenized tissue extract was stored at −80°C for long-term preservation or for future applications as required. Ferric-reducing ability of plasma (FRAP) assays evaluated the TAC of lung tissue. The lung tissue was isolated from the surrounding peri-lung tissue, followed by homogenization for the analysis. Specifically, the rinsing of the homogenized tissue (100 µL) was done with cold PBS (200 µL), and it was placed into a polyethylene tube (2 mL). Then, 10 µL of FRAP solution (Thermo Fisher Scientific Inc., Cat. No. EIAFECL2; Germany) was mixed with this mixture, followed by incubation for 15 min at 25°C. Afterward, centrifugation was done (12,000 *g*/10 min), and an ultraviolet (UV)–visible spectrophotometer measured the absorbance (Younis et al., 2023; Zhao et al., 2025).

Lung Tissue Lipid Peroxidation (LPO) Levels

Thiobarbituric acid reactive substances (TBARS) assays evaluated the LPO levels in lung tissue. In summary, the homogenized lung tissue (100 µL) was located into a polyethylene tube (2 mL), to which TBARS solution (100 µL; Invitrogen Inc., Catalog No. EEA021; Germany) was added. The mixture received incubation at 37°C for 30 min; then, a UV–visible spectrophotometer measured the absorbance (Younis et al., 2023).

Real-time Polymerase Chain Reaction (PCR) Assay

To extract total ribonucleic acid (RNA), TRIzol was mixed with lung tissue (60 mg), and then an incubation was done (2 min/25°C). The TRIzol/cell lysate processing was done according to the methods outlined by Zhou et al. (2018).

For complementary DNA (cDNA) synthesis from the total RNA extracted from the lung tissue, a commercial cDNA synthesis kit was applied as instructed. In summary, a reaction mixture was prepared that included total RNA (1,000 ng), 8 µL of deionized water, random and oligo primers (1 µL), and Takara Bio Mastermix (10 µL). This mixture was then placed in a thermal cycler, where cDNA templates were produced according to a specific temperature protocol: 10 min at 25°C, 45 min at 60°C, and a final 5 min at 60°C.

For the real-time PCR procedure, a reaction mixture was created using cDNA templates (1,000 ng), Takara Bio Mastermix (8 µL), and 1 µL of each of the forward and reverse primers. The ERK1/2, MEK1/2, Egr-1, and TF expression levels were quantified over 42 temperature cycles. The cycles included an annealing phase at 60°C for 1 min, a denaturation phase at 95°C for 30 s, and an extension phase at 72°C for 5 min. A melting curve analysis was performed through gently raising the temperature from 60°C to 95°C at 1°C per second. The cycle threshold (CT) values for the sample (S), control (C), and β-actin were noted and applied to calculate fold changes using the $2^{-\Delta\Delta CT}$ method. Primer-3 software designed the primers. β-Actin was the internal reference, and the sequences of the primers used are provided in Table 1 (Dai et al., 2022; Jiao et al., 2025).

$$\Delta\Delta CT = \left[\left(CT_S - Ct_{\beta\text{-actin}}\right) - \left(CT_S - CT_C\right)\right],$$

$$\text{Fold change of genes} = 2^{-\Delta\Delta CT}$$

P53 and Caspase-3 Positive Cells Detection

The detection of p53-positive cells and caspase-3 was used as an indicator for the lung parenchymal cells' apoptotic differentiation. Initially, lung tissues were rinsed with PBS, followed by standard processing that involved embedding the tissues in paraffin wax. Thin sections (5 µm) were then sliced from the paraffin blocks and placed onto slides, which underwent deparaffinization in xylene for 5–10 min, and then

Table 1. Primer Sequences.

Gene	Sequences (5′–3′)
β-Actin	Forward: AGGCATCCTCACCCTGAAGTA Reverse: CACACGCAGCTCATTGTAGA
ERK1/2	Forward: GAACTCCAAGGGCTATACCAAGT Reverse: GAGGGCAGAGACTGTAGGTAGT
MEK1/2	Forward: GCTTCTATGGTGCGTTCT Reverse: GAGTTGACTAGGATGTTGGA
Egr-1	Forward: GTCTGGGCGGGGGGGAGGGGA Reverse: GCCAGAACAGAGTGTCCTTTC
TF	Forward: GGTATCCGGTAGGTTGTTGGA Reverse: TTCCAGAGTGGAGGAAACTT

Note: Egr-1: Early growth response protein 1; TF: Tissue factor.

rehydration was done in a series of distilled/ethanol water solutions (100%, 95%, 70%, and 50% v/v) for 2–5 min each, ending with a 5-min rinse in distilled water. This entire deparaffinization and rehydration procedure was done in glass jars. Afterward, the samples received incubation at 95°C (24 h). Subsequently, they received hydrogen peroxide (0.3%) over 20 min, followed by incubation with primary antibodies against p53 and caspase-3 with dilutions of 1:1,000 from R&D Systems, Inc. (USA) at 25°C for 1 h. Tween-20 was employed as a wash buffer, while 5% (w/v) bovine serum albumin was used to block residual antibodies. Afterwards, a biotinylated secondary antibody was applied, followed by treatment with streptavidin-HRP for 60 minutes at room temperature. Rinsing of the sections with PBS and processing with 3,3′-diaminobenzidine for visualization was performed. The slides underwent counterstaining with hematoxylin. An Olympus light microscope examined the tissue sections, and images were captured at 100× (Model No. BX61TRF, Olympus, Japan). The percentage of p53-positive cells and Ki-67 to the overall cell count was calculated in 10 fields of view for each group, as described by Yu et al. (2018).

Lung Tissue Histopathology

Lung tissue was subjected to standard processing procedures, and sections (5 μm) were sliced from paraffin wax blocks, followed by staining with hematoxylin and eosin (H&E). Histopathological characteristics, including those of the pulmonary artery, bronchus, bronchioles, and alveoli, were examined by a BX61TRF light microscope (Olympus, Japan) linked to ImageJ software for analysis (Eriksson et al., 2020).

Tissue Preparation and Stereological Measurements

Immersion techniques were utilized to assess the initial volumes of the lung tissues. Following the estimation of tissue shrinkage rates, isotropic uniform random (IUR) sections were created using the orientation approach. Following processing of the tissue, paraffin blocks were formed, from which sections (5 μm) were sliced using a Leica Microsystems instrument. These tissue sections received stained with H&E.

To determine tissue shrinkage, the ultimate diameter of the circular section was assessed following processing and applied in the equation below:

$$\text{Volume shrinkage} = 1 - \left(\frac{\text{AA}}{\text{AB}}\right)^{1.5}$$

The volume density of the targeted structures—air parenchyma volume (APV), tissue parenchyma volume (TPV), lung volume (LV), and vessel volume (VV)—was assessed on sections (5 μm) using the point-counting approach in conjunction with Delesse's equation.

$$Vv(\text{structure}) = \frac{\sum_{i=1}^{n} p(\text{structure})}{\sum_{i=1}^{n} (\text{reference})}$$

"$\sum_{i=1}^{n} p(\text{structure})$" indicates the number of test points that settled on the target structures, and "$\sum_{i=1}^{n} p$" is the overall number of points that fell on the lung sections. The equation below determines the total targeted structural volume (Akbaribazm et al., 2020).

$$V(\text{structure}) = V(\text{total lung}) \times Vv(\text{structure})$$

Transmission Electron Microscopic (TEM) Study

For TEM analysis, multiple lung tissue samples measuring 1 mm³ were fixed in a 2.5% glutaraldehyde solution in phosphate buffer for 48 h. Following this, the specimens received 1% osmium tetroxide for 1 h and then underwent dehydration by a series of ethanol concentrations ranging from 50% to 100%. Semi-thin sections (0.5–1 μm) were sliced from the blocks and stained using toluidine blue. A light microscope was used to identify specific areas of interest. Subsequently, ultrathin sections (60 nm) were prepared and stained with a saturated solution of lead citrate and uranyl acetate. These sections were evaluated using a JEOL-JEM-100 SX electron microscope (JEOL Co. Inc., Japan) functioning at 80 kV, and images were captured with an iTEM MegaView digital camera (Olympus Soft Imaging Solutions, Germany) (Hopfer et al., 2021).

Data Analysis

Statistical Package for the Social Sciences (SPSS) 16.0 conducted statistical analyses, employing one-way analysis of variance (ANOVA) and Duncan's test, with a significance level established at $p < .05$. The data normality was evaluated using the Kolmogorov–Smirnov test, where $p > .05$ suggested a normal distribution. Values are reported as means ± standard deviations (SD).

Results

LD_{50} of CYN

Lorek's method conducted the LD_{50} evaluation of the groups $\left[\text{LD}_{50} = (\text{A} \times \text{B})\ ½\right]$ for CYN, and following 24 h, the LD_{50} was 200 mg/kg (where A is the lowest concentration that induced toxicity) and 100 mg/kg (where B is the highest concentration without fatalities or toxicity). Applying these values to Lorek's formula, the LD_{50} for CYN was 141.42 mg/kg. Consequently, doses below 141.42 mg/kg were deemed safe for administration.

Body and Lung Weight

The PE group demonstrated a notable elevation in both lung and body weight versus the sham group ($p < .05$). Conversely, the PE + 10 CYN group exhibited lower values for both weight measures than the PE group, with the decrease in body weight being significant ($p < .05$). Furthermore, CYN significantly reduced both body and lung weight in the PE + 25 CYN group in comparison to the PE group ($p < .05$) (Figure 1).

Serum MCP-1, TF, IL-6, VCAM-1, IL-1β, and ICAM-1 Concentrations

Serum concentrations of inflammatory cytokines (IL-6, IL-1β) and VCAM-1, MCP-1, TF, and ICAM-1 were significantly enhanced in the PE group, in comparison to the sham group ($p < .05$). In the PE + 10 CYN group, CYN significantly reduced the serum TF, IL-6, VCAM-1, IL-1β, MCP-1, and ICAM-1 concentrations versus the PE group ($p < .05$). The PE + 25 CYN group displayed the most pronounced decrease, with significantly lower serum concentrations of the inflammatory cytokines and other pro-inflammatory endothelial factors versus the PE group (Figure 2a and 2b).

Lung Tissue TBARS and FRAP Concentrations

There was a significant reduction in FRAP and TBARS levels in the PE group in comparison to the sham group ($p < .05$).

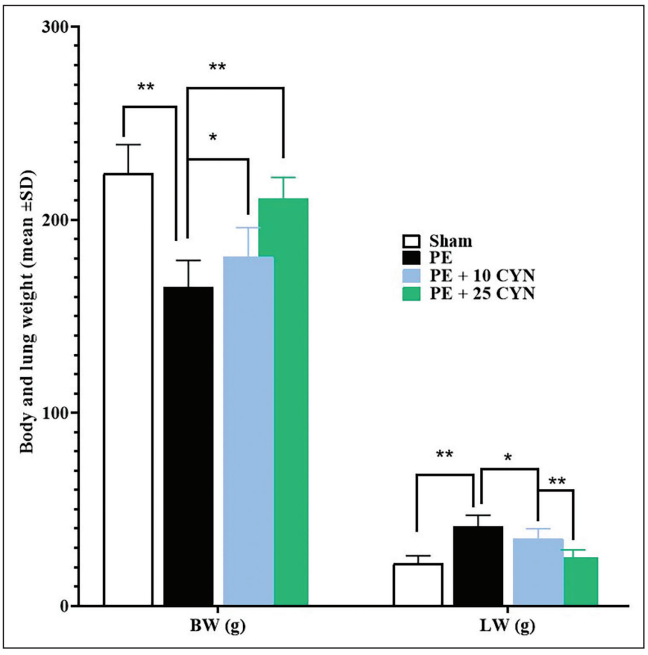


Figure 1. The Weights of the Whole Animal's Body Weight (BW) and of Lung Weight (LW) in the Different Experimental Groups.

Note: Data are given as means ± standard deviation (SD). n = 10/group. $^{*}p < .05$ and $^{**}p < .01$.

However, the PE + 10 CYN group showed a marked elevation in the two OS parameters. The PE + 25 CYN group exhibited significantly higher levels of TBARS and FRAP ($p < .05$) in comparison to the PE group (Figure 3).

Expression of Lung ERK1/2, MEK1/2, Egr-1, and TF Genes

Upon evaluating the gene expression results for the MEK/ERK/Egr-1/TF pathway, it was observed that this pathway was activated following PE, with significant increases in the expression of all four genes (MEK1/2, ERK1/2, Egr-1, and TF) versus the sham group. CYN significantly reduced ($p < .05$) the Egr-1, MEK1/2, ERK1/2, and TF expression levels in both the PE + 10 CYN and PE + 25 CYN groups relative to the PE group (Figure 4).

Immunohistochemistry (IHC) Findings

The caspase-3 and p53 expression in lung parenchymal cells was notably higher ($p < .05$) in the PE group versus the sham group. In the PE + 10 CYN group, the levels of p53 and caspase-3 were lower than in the PE group; nonetheless, these differences were not significant ($p > .05$). Conversely, CYN reduced the p53 and caspase-3 expression dose dependently in the PE + 25 CYN group versus the PE group (Figures 5–7).

Stereological Findings

The PE group showed a notable elevation ($p < .05$) in LV, TPV, and VV, along with a significant reduction ($p < .05$) in APV versus the sham group. In the PE + 25 CYN group, CYN significantly reduced lung tissue LV, TPV, and VV, while significantly increasing APV versus the PE group ($p < .05$). Compared to the sham group, there was enhanced lymphocyte infiltration, decreased alveolar space, and signs of alveolar degeneration in the PE group. This group exhibited evident congestion in the vessels and alveoli, with the alveolar parenchymal space and vessels filled with red blood cells (RBCs). In contrast, the CYN-treated groups showed a dose-dependent reduction in lymphocyte infiltration, and the alveolar space appeared normal and uniform. Additionally, vascular and alveolar congestion were not found in the CYN-treated groups (Figure 8a and 8b).

TEM Findings

Electron micrographs of the interalveolar septum in the PE group, compared to the sham group, revealed irregular thickening and interruptions in some areas of the basement membrane of type 1 pneumocytes. In the interalveolar septum of the PE group, type 2 pneumocytes exhibited shrunken nuclei (N), swollen mitochondria (M), an increased number of lysosomes, and apoptotic vesicles adjacent to large, irregular heterochromatic nuclei. In the groups treated with CYN (mainly

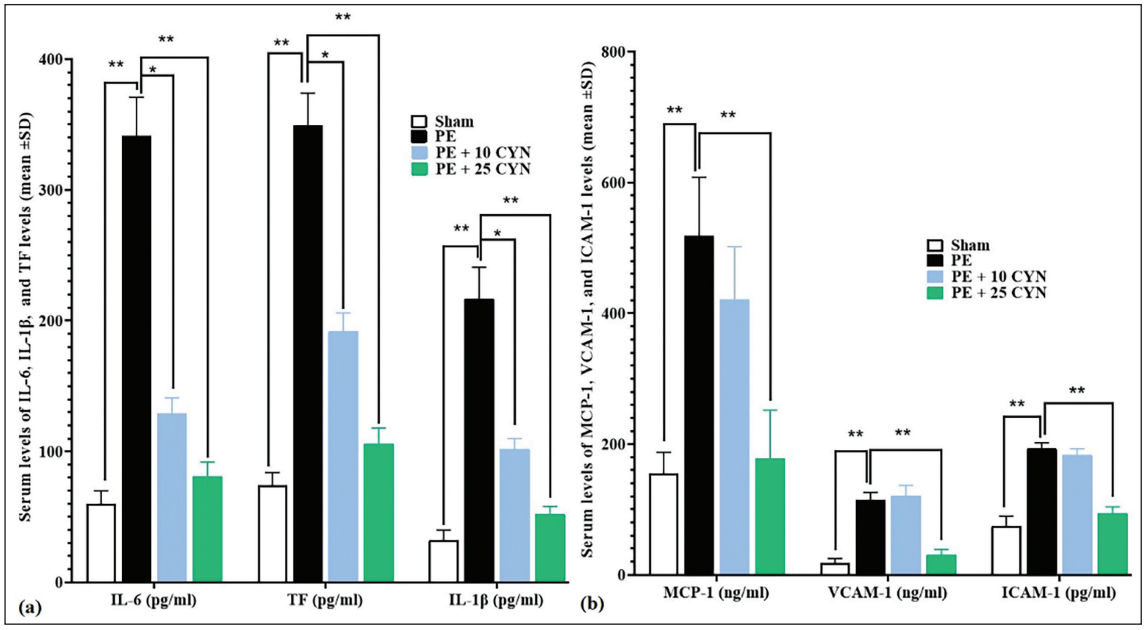


Figure 2. (a) The Mean Serum Levels of Interleukin-6 (IL-6), Tissue Factor (TF), and Interleukin-1 Beta (IL-1β) (pg/mL) and (b) Mean Serum Levels of Monocyte Chemoattractant Protein-1 (MCP-1), Vascular Cell-adhesion Molecule-1 (VCAM-1) (ng/mL), and Intercellular Adhesion Molecule-1 (ICAM-1) (pg/mL) in the Different Experimental Groups.

Note: Data are given as means ± standard deviation (SD). n = 10/group. $^{*}p < .05$ and $^{**}p < .01$.

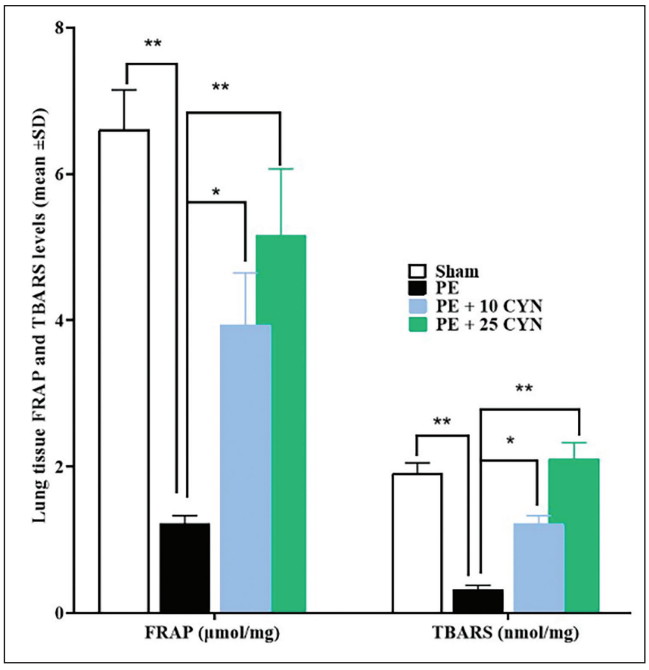


Figure 3. The Mean Lung Tissue Levels of Ferric Reducing Ability of Plasma (FRAP) (µmol/mg Protein) and Thiobarbituric Acid Reactive Substances (TBARS) (nmol/mg Proteins) in the Different Experimental Groups.

Note: Data are given as means ± standard deviation (SD). n = 10/group. $^{*}p < .05$ and $^{**}p < .01$.

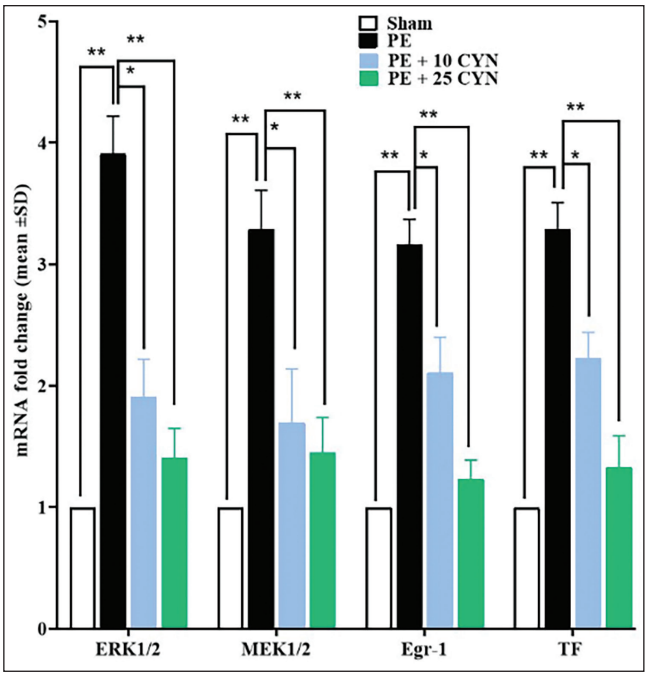


Figure 4. The Mean Lung Tissue Expression of ERK1/2, MEK1/2, Early Growth Response Protein 1 (Egr-1), and Tissue Factor (TF) Genes Expression in the Different Experimental Groups.

Note: Data are given as means ± standard deviation (SD). n = 10/group. $^{*}p < .05$ and $^{**}p < .01$.

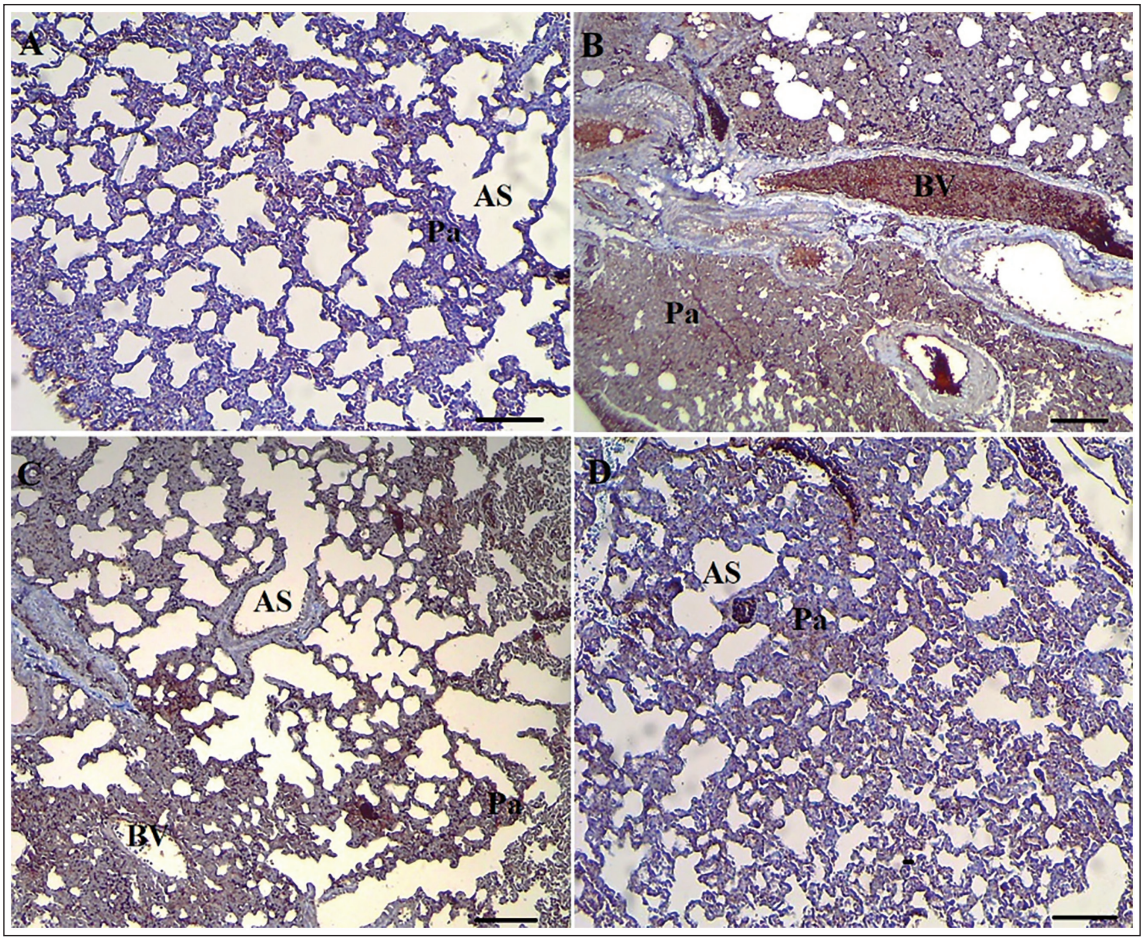


Figure 5. (A–D) Representative Micrographs Illustrating the Immunohistochemical Staining of Caspase-3 Positive Cells in the Various Experimental Groups.

Notes: AS: Alveolar space; BV: Blood vessels; Pa: Parenchyma. 3,3′-Diaminobenzidine (DAB) staining. Original magnification ×100. Scale bar: 100 μm. (A) Sham, (B) pulmonary embolism (PE), (C) PE + 10 cynaropicrin (CYN), and (D) PE + 25 CYN.

PE + 25 CYN), both type 1 and type 2 pneumocytes displayed normal, rounded euchromatic nuclei, no apoptotic vesicles, few lysosomes, and an intact basement membrane (Figure 9).

Discussion

This study showed that CYN mitigated cell apoptosis induced by PE, potentially linked to its ability to inhibit inflammatory responses, reduce OS, and suppress the MEK/ERK/Egr-1/TF signaling pathway involved in the PE process. In a rat model of CTEPH, we further confirmed CYN's effects on both the lung parenchymal structure and its ultrastructure. We observed that CYN lowered the levels of inflammatory cytokines, chemokines, and adhesion molecules in the peripheral blood, reducing apoptosis. These findings indicate that CYN may be a promising therapeutic option for CTEPH.

CYN is a natural sesquiterpene lactone primarily found in artichokes and other plants within the Asteraceae family. It is recognized for its wide range of biological activities, including anti-inflammatory, antioxidant, anti-thrombotic, cytoprotective, and anti-microbial properties (De Cicco et al., 2021). CYN is noted for its potential therapeutic benefits in cardiovascular diseases, attributed to its antioxidant effects, ability to activate anti-platelet mechanisms, and anti-inflammatory actions, which involve scavenging reactive oxygen species (ROS), inhibiting cyclooxygenases, and activating various anti-inflammatory pathways (Gonçalves et al., 2023). Animal studies involving rats and mice indicate that during CTEPH, the pathways associated with OS induction (PI3K/AKT) and apoptosis induction (Nrf2/NF-kB) are significantly affected (Chen et al., 2023). In the rat model of CTEPH, flavonoid compounds were found to reduce atelectasis and pulmonary emphysema through systemic gavage and local inhalation, ultimately enhancing respiratory capacity (Jung et al., 2023). In the present study, CYN also preserved the respiratory parenchyma and alveolar space by inhibiting inflammatory pathways, thereby

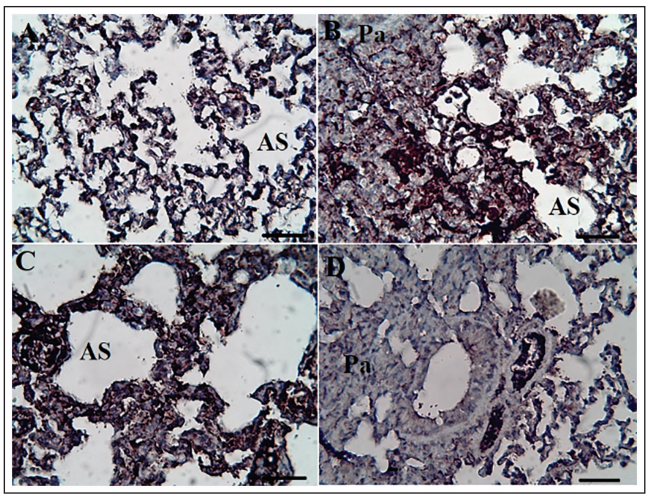


Figure 6. (A–D) Representative Micrographs Illustrating the Immunohistochemical Staining of p53-positive Cells in the Various Experimental Groups.

Notes: AS: Alveolar space; BV: Blood vessels; Pa: Parenchyma. 3,3′-Diaminobenzidine (DAB) staining. Original magnification ×400. Scale bar: 25 μm. (A) Sham, (B) pulmonary embolism (PE), (C) PE + 10 cynaropicrin (CYN), and (D) PE + 25 CYN.

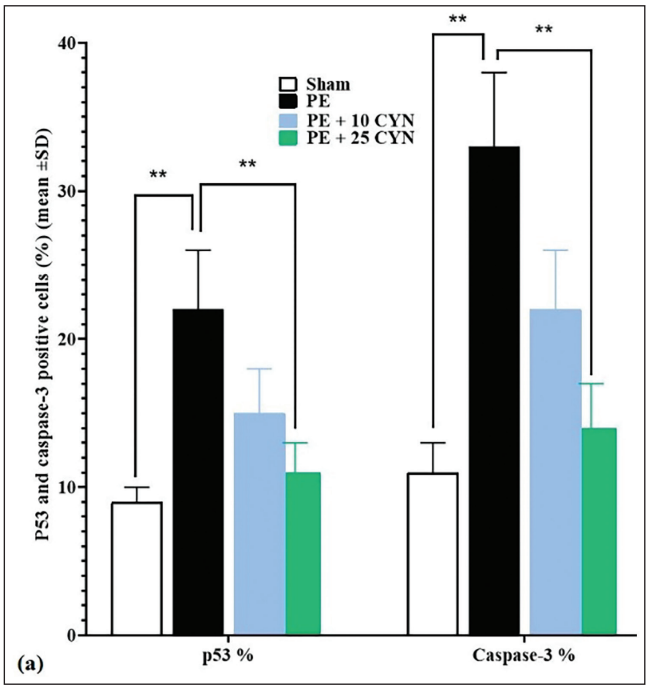


Figure 7. The Mean Lung Tissue p53 and Caspase-3 Positive Cells (%).

Note: Data are given as means ± standard deviation (SD). n = 10/group. $^{*}p < .05$ and $^{**}p < .01$.

protecting against parenchymal emphysema and atelectasis (Casper, 2023). Furthermore, CYN serves as a potent antagonist of phosphodiesterase, decreasing the contractility of vascular smooth muscle cells in a PDE1-dependent manner, thereby helping to alleviate hypertension. CYN also decreases insulin resistance by downregulating enzymes that generate free radicals while enhancing the activity of those that scavenge ROS (Chen et al., 2023; Jin & Leng, 2023). In this study, we aimed to explore the roles of CYN in CTEPH by assessing various biochemical parameters.

MCP-1, a crucial factor in promoting the infiltration of inflammatory cells into the lungs, is known to be expressed in all pulmonary artery walls following pulmonary thromboembolism (Mulholland et al., 2019). Additionally, VCAM-1 and ICAM-1, which are inflammatory mediators released by endothelial cells, facilitate the infiltration of inflammatory cells into the pulmonary artery tissue. Furthermore, TF, a pro-coagulant protein, is significantly upregulated during thrombosis and acts as a membrane-bound initiator of the extrinsic coagulation pathway (Habas & Shang, 2018). Studies have shown that monocyte and plasma TF levels are markedly elevated in patients with deep vein thrombosis (DVT) compared to healthy controls. Moreover, research indicates that plasma levels of IL-6 and IL-1β, produced by leukocytes, are increased and contribute to the pathogenesis of PE in affected patients (Miao et al., 2018). Experimental studies in mice have demonstrated that circulating mononuclear phagocytes carrying TF, along with MCP-1, and neutrophils expressing ICAM-1, play a significant role in thrombus formation. In the present study, we demonstrated that CYN effectively reduced the production of pro-inflammatory cytokines IL-6 and IL-1β, which are involved in vascular thrombosis (Hofbauer et al., 2020). Our findings also indicated that CYN possesses anti-thrombotic effects, preventing the formation of disseminated thrombi by inhibiting key mediators of thrombus formation, including TF, MCP-1, VCAM-1, and ICAM-1. This suggests its potential role in the treatment of PE.

The MEK/ERK signaling pathway, part of the MAPK cascade, is essential for transmitting signals from growth factors and hormones to the nucleus, influencing cell proliferation, differentiation, and survival. Key components include MEK, which activates ERK, and Egr-1, a transcription factor that regulates gene expression in response to stimuli (Yang et al., 2019). This pathway is activated by pro-inflammatory factors, leading to increased expression of the pro-coagulant TF, promoting thrombosis. Additionally, it plays a vital role in vascular smooth muscle cell proliferation and migration for vascular repair. It supports angiogenesis by activating endothelial cells with growth factors like VEGF (Jung et al., 2023). The MEK/ERK pathway also interacts with other signaling pathways, enhancing responses to growth factors and inflammation, while regulating various genes involved in inflammation and vascular remodeling (Zhao et al., 2024). In the present study, it was found that the enhanced MEK/ERK/Egr-1/TF signaling pathway facilitates the progression of PE during CTEPH. Conversely, CYN inhibited this pathway, reducing TF and the mechanisms associated with CTEPH. The findings indicated that CYN provided structural

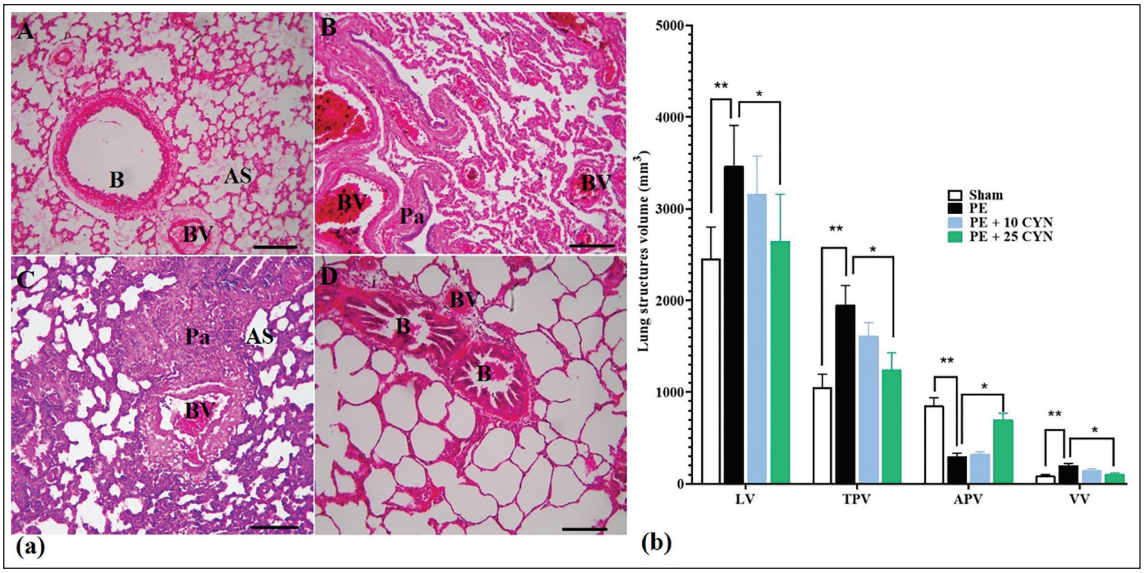


Figure 8. (a) A–D: Representative Micrographs Illustrating Alveolar Space (AS), Parenchyma (Pa), Bronchioles (B), and Blood Vessels (BV) in Lung Tissues in the Different Experimental Groups. Hematoxylin and Eosin (H&E) Staining. Original Magnification ×100. Scale Bar: 100 μm. (A) Sham, (B) Pulmonary Embolism (PE), (C) PE + 10 Cynaropicrin (CYN), and (D) PE + 25 CYN. (b) Mean Levels of Stereological Parameters in Lung Tissue in the Different Experimental Groups. Lung Volume (LV), Tissue Parenchyma Volume (TPV), Air Parenchyma Volume (APV), and Vessel Volume (VV).

Note: Data are given as means ± standard deviation (SD). n = 10/group. $^{*}p < .05$ and $^{**}p < .01$.

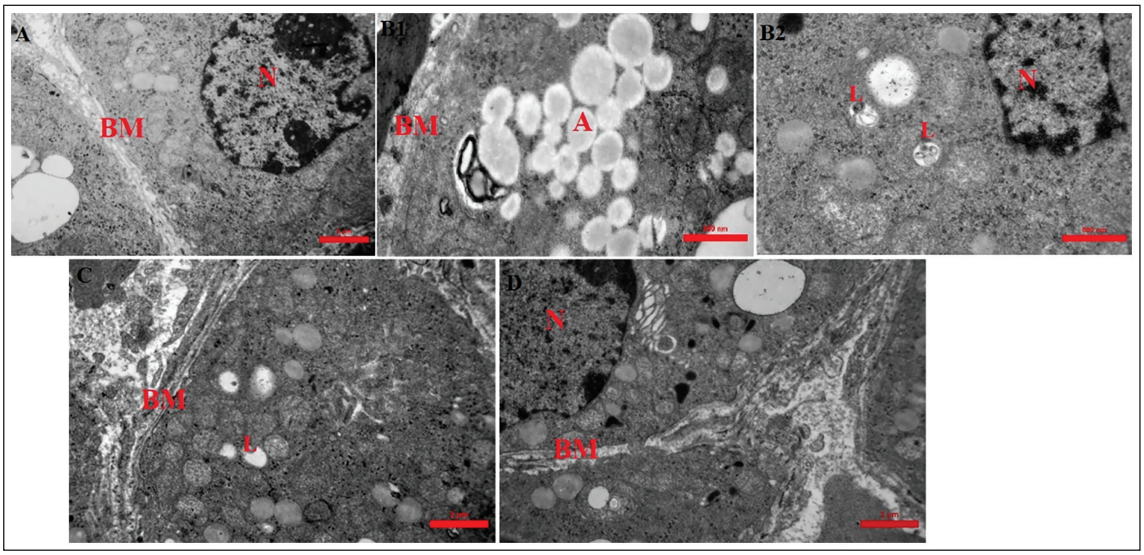


Figure 9. Transmission Electron Microscopic (TEM) Micrographs of the Lung Tissue in the Different Experimental Groups. (A) Sham (Scale Bar: 2 μm), (B) Pulmonary Embolism (PE) (B1, Scale Bar: 300 nm; B2, Scale Bar: 800 nm), (C) PE + 10 Cynaropicrin (CYN) (Scale Bar: 2 μm), and (D) PE + 25 CYN (Scale Bar: 2 μm).

Note: AV: Apoptotic vesicles; BM: Basement membrane; L: Lysosome; N: Nucleus.

protection to the lung parenchyma by inhibiting mitochondrial apoptotic pathways in monocyte cells, specifically reducing levels of p53 and caspase-3 after mitigating the effects of CTEPH. These changes contributed to the preservation of lung parenchyma, ultimately helping to maintain respiratory space volume and reduce the parenchymal damage between the alveolar septa. Our future research will primarily concentrate on CYN in other models of CTEPH and intimal tissue samples to replicate studies involving endarterectomized samples from patients with CTEPH.

Conclusion

Our research indicates that CYN has substantial therapeutic effects in a rat model of PE, primarily by reducing inflammatory responses and inhibiting the MEK/ERK/Egr-1/TF signaling pathway. The decrease in key inflammatory biomarkers and the inhibition of apoptotic pathways highlight CYN's potential as a treatment for PE. However, there are limitations to our study, including the need for further molecular investigations to confirm these results, both *in vivo* and *in vitro*. Additionally, the safety and efficacy of CYN must be thoroughly evaluated in human subjects to determine its clinical applicability.

Abbreviations

CTEPH: Chronic thromboembolic pulmonary hypertension; CYN: Cynaropicrin; Egr-1: Early growth response protein 1; FRAP: Ferric reducing ability of plasma; ICAM-1: Intercellular adhesion molecule-1; IL-6: Interleukin-6; IL-1β: Interleukin-1 beta; LD_{50}: Lethal dose 50; MAPK: Mitogen-activated protein kinase; MCP-1: Monocyte chemoattractant protein-1; NF-κB: Nuclear factor kappa-light-chain-enhancer of activated B cells; Nrf2: Nuclear factor erythroid 2-related factor 2; OD: Optical density; PASMCs: Pulmonary artery smooth muscle cells; PE: Pulmonary embolism; PH: Pulmonary hypertension; qPCR: Quantitative real-time PCR; Real-time PCR: Real-time polymerase chain reaction; ROS: Reactive oxygen species; SIRT1: Sirtuin 1; TAC: Total antioxidant capacity; TBARS: Thiobarbituric acid reactive substances; TF: Tissue factor; VCAM-1: Vascular cell-adhesion molecule-1.

Consent for Publications

All authors read and approved the final manuscript for publication.

Declaration of Conflicting Interests

The authors declared no potential conflicts of interest with respect to the research, authorship, and/or publication of this article.

Ethical Approval

The experimental protocols of this study were approved by the Hospital of Shaoxing University ethics committee.

Funding

The authors received no financial support for the research, authorship, and/or publication of this article.

Informed Consent

Not applicable.

ORCID iD

Mingliang Wu https://orcid.org/0009-0004-5210-5231

References

Akbaribazm, M., Khazaei, M. R., & Khazaei, M. (2020). *Trifolium pratense* L. (red clover) extract and doxorubicin synergistically inhibits proliferation of 4T1 breast cancer in tumor-bearing BALB/c mice through modulation of apoptosis and increase antioxidant and anti-inflammatory related pathways. *Food Science and Nutrition*, *8*(8), 4276–4290. https://doi.org/10.1002/fsn3.1724

Barbosa, R., Acevedo, L. A., & Marmorstein, R. (2021). The MEK/ERK network as a therapeutic target in human cancer. *Molecular Cancer Research*, *19*(3), 361–374. https://doi.org/10.1158/1541-7786.MCR-20-0687

Casper, E. (2023). The crosstalk between Nrf2 and NF-κB pathways in coronary artery disease: Can it be regulated by SIRT6? *Life Sciences*, 330, Article 122007. https://doi.org/10.1016/j.lfs.2023.122007

Chen, L., Ye, T., Wang, X., Han, L., Wang, T., Qi, D., & Cheng, X. (2023). The mechanisms underlying the pharmacological effects of GuiPi decoction on major depressive disorder based on network pharmacology and molecular docking. *Combinatorial Chemistry and High Throughput Screening*, *26*(9), 1701–1728. https://doi.org/10.2174/1386207325666220831152959

Dai, H., Hu, W., Zhang, L., Jiang, F., Mao, X., Yang, G., & Li, L. (2021). FGF21 facilitates autophagy in prostate cancer cells by inhibiting the PI3K–Akt–mTOR signaling pathway. *Cell Death & Disease, 12*(4), 303. https://doi.org/10.1038/s41419-021-03588-w

Dai, Y., Zhou, Q., Liu, Y., Chen, X., Li, F., Yu, B., Zhang, Y., & Kou, J. (2022). Ruscogenin alleviates deep venous thrombosis and pulmonary embolism induced by inferior vena cava stenosis inhibiting MEK/ERK/Egr-1/TF signaling pathway in mice. *Current Pharmaceutical Design*, *28*(24), 2001–2009. https://doi.org/10.2174/1381612828666220526120515

De Cicco, P., Busà, R., Ercolano, G., Formisano, C., Allegra, M., Taglialatela-Scafati, O., & Ianaro, A. (2021). Inhibitory effects of cynaropicrin on human melanoma progression by targeting MAPK, NF-κB, and Nrf-2 signaling pathways in vitro. *Phytotherapy Research*, *35*(3), 1432–1442. https://doi.org/10.1002/ptr.6906

Dibua, M. U., Garba, D. E., Elechenu, E. C., Emencheta, S. C., & Okeke, E. S. (2022). Assessment of acute toxicity, LD_{50} and histopathological evaluation of *Nigella sativa* and *Moringa oleifera* seed extracts in Wistar rats. *Tropical Journal of Natural Product Research*, *6*(11), 1840–1843.

Eriksson, J., Sjögren, E., Lennernäs, H., & Thörn, H. (2020). Drug absorption parameters obtained using the isolated perfused rat lung model are predictive of rat *in vivo* lung absorption. *The AAPS Journal*, *22*(3), 71. https://doi.org/10.1208/s12248-020-00456-x

Freund, Y., Cohen-Aubart, F., & Bloom, B. (2022). Acute pulmonary embolism: A review. *JAMA*, *328*(13), 1336–1345. https://doi.org/10.1001/jama.2022.16815

Gao, H., Zhang, Q., Chen, J., Cooper, D. K. C., Hara, H., Chen, P., Wei, L., Zhao, Y., Xu, J., Li, Z., Cai, Z., Luan, S., & Mou, L. (2018). Porcine IL-6, IL-1β, and TNF-α regulate the expression of pro-inflammatory-related genes and tissue factor in human umbilical vein endothelial cells. *Xenotransplantation*, *25*(5), Article e12408. https://doi.org/10.1111/xen.12408

Gonçalves, A., Sampaio, C. I., Ševčovičová, A., Dias, A. M., & Oliveira, R. (2023). Cynaropicrin-and chlorogenic acid-rich extracts easily prepared from *Cynara cardunculus* var. *scolymus*: Antioxidant and antigenotoxic properties. *Biocatalysis and Agricultural Biotechnology*, 52, Article 102808. https://doi.org/10.1016/j.bcab.2023.102808

Habas, K., & Shang, L. (2018). Alterations in intercellular adhesion molecule 1 (ICAM-1) and vascular cell adhesion molecule 1 (VCAM-1) in human endothelial cells. *Tissue and Cell*, *54*, 139–143. https://doi.org/10.1016/j.tice.2018.09.002

Hofbauer, T. M., Ondracek, A. S., Mangold, A., Scherz, T., Nechvile, J., Seidl, V., Brostjan, C., & Lang, I. M. (2020). Neutrophil extracellular traps induce MCP-1 at the culprit site in ST-segment elevation myocardial infarction. *Frontiers in Cell and Developmental Biology*, 8, Article 564169. https://doi.org/10.3389/fcell.2020.564169

Hopfer, H., Herzig, M. C., Gosert, R., Menter, T., Hench, J., Tzankov, A., Hirsch, H. H., & Miller, S. E. (2021). Hunting coronavirus by transmission electron microscopy—A guide to SARS-CoV-2-associated ultrastructural pathology in COVID-19 tissues. *Histopathology*, *78*(3), 358–370. https://doi.org/10.1111/his.14264

Jiao, X., Zhang, Q., Ye, G., Xing, F., Xie, D., & Wang, L. (2025). Protective effects of apricot kernel oil and metformin against BPA-induced ovarian toxicity in rat models of polycystic ovary syndrome: Insights into PI3K/AKT and mitochondrial apoptosis pathways. *Toxicology Research*, *14*(3), tfaf071. https://doi.org/10.1093/toxres/tfaf071

Jin, T., & Leng, B. (2023). Cynaropicrin averts the oxidative stress and neuroinflammation in ischemic/reperfusion injury through the modulation of NF-kB. *Applied Biochemistry and Biotechnology*, *195*(9), 5424–5438. https://doi.org/10.1007/s12010-022-04060-x

Jung, E., Ou, S., Ahn, S. S., Yeo, H., Lee, Y. H., & Shin, S. Y. (2023). The JNK-EGR1 signaling axis promotes TNF-α-induced endothelial differentiation of human mesenchymal stem cells via VEGFR2 expression. *Cell Death and Differentiation*, *30*(2), 356–368. https://doi.org/10.1038/s41418-022-01088-8

Kim, N. H., Delcroix, M., Jais, X., Madani, M. M., Matsubara, H., Mayer, E., Ogo, T., Tapson, V. F., Ghofrani, H.-A., & Jenkins, D. P. (2019). Chronic thromboembolic pulmonary hypertension. *The European Respiratory Journal*, *53*(1), Article 1801915. https://doi.org/10.1183/13993003.01915-2018

Li, X.-C., Zhu, X.-Y., Wang, Y.-Y., Tong, S.-L., Chen, Z.-L., Lu, Z.-Y., Zhang, J.-H., Song, L.-L., Wang, X.-H., Zhang, C., Sun, Y.-H., Zhong, C.-Y., Su, L.-H., Wang, L.-X., & Huang, X.-Y. (2024). Canagliflozin alleviates pulmonary hypertension by activating PPARγ and inhibiting its S225 phosphorylation. *Acta Pharmacologica Sinica*, *45*(9), 1861–1878. https://doi.org/10.1038/s41401-024-01286-9

Liu, Y.-Y., Zhang, W.-Y., Zhang, M.-L., Wang, Y.-J., Ma, X.-Y., Jiang, J.-H., Wang, R., & Zeng, D.-X. (2022). DNA-PKcs participated in hypoxic pulmonary hypertension. *Respiratory Research*, *23*(1), 246. https://doi.org/10.1186/s12931-022-02171-x

Matos, M. S., Anastácio, J. D., & Nunes dos Santos, C. (2021). Sesquiterpene lactones: Promising natural compounds to fight inflammation. *Pharmaceutics*, *13*(7), 991. https://doi.org/10.3390/pharmaceutics13070991

Mercier, O., Dubost, C., Delaporte, A., Genty, T., Fabre, D., Mitilian, D., Girault, A., Issard, J., Astaneh, A., Menager, J.-B., Dauriat, G., Mussot, S., Jevnikar, M., Jais, X., Humbert, M., Simonneau, G., Dartevelle, P., Ion, I., Stephan, F., … Fadel, E. (2022). Pulmonary thromboendarterectomy: The Marie Lannelongue Hospital experience. *Annals of Cardiothoracic Surgery*, *11*(2), 143–150. https://doi.org/10.21037/acs-2021-pte-20

Miao, W., Zhao, K., Deng, W., & Teng, J. (2018). Coagulation factor hyperfunction after subarachnoid hemorrhage induces deep venous thrombosis. *World Neurosurgery*, *110*, e46–e52. https://doi.org/10.1016/j.wneu.2017.09.200

Mulholland, B. S., Forwood, M. R., & Morrison, N. A. (2019). Monocyte chemoattractant protein-1 (MCP-1/CCL2) drives activation of bone remodelling and skeletal metastasis. *Current Osteoporosis Reports*, *17*(6), 538–547. https://doi.org/10.1007/s11914-019-00545-7

Porro, C., Benameur, T., Cianciulli, A., Vacca, M., Chiarini, M., De Angelis, M., & Panaro, M. A. (2024). Functional and therapeutic potential of *Cynara scolymus* in health benefits. *Nutrients*, *16*(6), 872. https://doi.org/10.3390/nu16060872

Salekzamani, S., Ebrahimi-Mameghani, M., & Rezazadeh, K. (2019). The antioxidant activity of artichoke (*Cynara scolymus*): A systematic review and meta-analysis of animal studies. *Phytotherapy Research*, *33*(1), 55–71. https://doi.org/10.1002/ptr.6213

Wu, D., Chen, Y., Wang, W., Li, H., Yang, M., Ding, H., Lv, X., Lian, N., Zhao, J., & Deng, C. (2020). The role of inflammation in a rat model of chronic thromboembolic pulmonary hypertension induced by carrageenan. *Annals of Translational Medicine*, *8*(7), 492. https://doi.org/10.21037/atm.2020.02.86

Yang, J., Sun, L., Han, J., Zheng, W., & Peng, W. (2019). DUSP1/MKP-1 regulates proliferation and apoptosis in keratinocytes through the ERK/Elk-1/Egr-1 signaling pathway. *Life Sciences*, *223*, 47–53. https://doi.org/10.1016/j.lfs.2019.03.018

Ye, H., Wang, K., & Li, K. (2023). Anti-osteoporosis effect of cynaropicrin against ovariectomy-induced osteoporosis in rats. *Pharmacognosy Magazine*, *19*(2), 448–460. https://doi.org/10.1177/09731296221137415

Younis, T., Jabeen, F., Hussain, A., Rasool, B., Raza Ishaq, A., Nawaz, A., El-Nashar, H. A. S., & El-Shazly, M. (2023). Antioxidant and pulmonary protective potential of *Fraxinus xanthoxyloides* bark extract against CCl_4-induced toxicity in rats. *Chemistry and Biodiversity*, *20*(3), Article e202200755. https://doi.org/10.1002/cbdv.202200755

Yu, X.-Y., Zhang, X.-W., Wang, F., Lin, Y.-B., Wang, W.-D., Chen, Y.-Q., Zhang, L.-J., & Cai, L. (2018). Correlation and prognostic significance of PD-L1 and P53 expression in resected primary pulmonary lymphoepithelioma-like carcinoma. *Journal of Thoracic Disease*, *10*(3), 1891–1902. https://doi.org/10.21037/jtd.2018.03.14

Zaker-Esteghamati, H., Seidavi, A., & Bouyeh, M. (2021). Effect of *Cynara scolymus* and its derivatives on broilers: An updated review. *Animal Biotechnology*, *32*(5), 656–662. https://doi.org/10.1080/10495398.2020.1737097

Zhao, R., Xu, S., Jia, C., Zhu, S., Ma, L., Chen, Y., & Chen, D. (2025). Exploring the protective role of *Heracleum persicum* L. extract in testicular toxicity induced by mercuric chloride: Insights into hormonal modulation and cell survival pathways. *Toxicology Research*, *14*(1), tfaf015. https://doi.org/10.1093/toxres/tfaf015

Zhao, S., Zhou, J., Chen, R., Zhou, W., Geng, H., Huang, Y., Shi, S., Yuan, L., Wang, Z., & Wang, D. (2024). Decreased FGF23 inhibits placental angiogenesis via the ERK1/2-EGR-1 signaling pathway in preeclampsia. *Cytokine*, 176, Article 156508. https://doi.org/10.1016/j.cyto.2024.156508

Zhou, W., Chen, X., Hu, Q., Chen, X., Chen, Y., & Huang, L. (2018). Galectin-3 activates TLR4/NF-κB signaling to promote lung adenocarcinoma cell proliferation through activating lncRNA-NEAT1 expression. *BMC Cancer*, *18*(1), 580. https://doi.org/10.1186/s12885-018-4461-z